Ascertaining Abnormal Regions in Mammogram Images Using Gravitational Search Local Map View Technique

M.P. Sukassini, T.Velmurugan

Abstract: Segmentation of mammogram images has gained importance in many medical treatments and diagnostic processes. Mammogram image segmentation aims at correctly separating different tissues, organs, or pathologies in volumetric image data. Most of the existing algorithms for image segmentation have a "scattered" cluster problem (disconnected clusters) happened in many clustering techniques (agglomerative, k-means, Dbscan) . Above algorithms not taken into account of both quality value and connectivity of points and region varying shapes. Two methods are proposed in this paper. The first technique is LMV (Local Map View) and the second technique is GSLMV (Gravitational Search Local Map View). LMV concentrates on determination of local quality for each point in all instances of the region in the comparative similarity view by applying the initial cluster technique. This view allows the user to choose instances for detailed analysis and filter the outlier instances from the input, next specific feature selection process identifies regions with systematic characteristics across the images. In this research work, pixels in groups with high intensity are assumed to be abnormal regions in cancer and non-cancer images. Fuzzy clustering is used to cluster the pixels. The optimal threshold from GS are initialized as cluster centres. This increases the speed of GSLMV algorithm. Performances of GSA, LMV and GSLMV methods are measured using False Rejection Rate, pixel count, Peak signal to noise ratio and runtime metrics. GSLMV showed better results based on pixel count, PSNR and runtime.

Index Terms: Mammogram image, Segmentation, Local Map View, Peak to Signal Noise Ratio, Gravitational Search Algorithm.

I. INTRODUCTION

Innovations of science and technology made human life simpler by reducing human burden, but at the same time it has changed human life style and health with negative effects. It made human infirm by affecting with different ailment. Among this the most common disease is cancer. Cancer is a malady in which cells are developed out of control. Breast cancer is the most common cancer in women. Breast cancer death rate has been deteriorated over time, but remains the second foremost source of death among women. Cancer is staged according to the size of the tumour. In stage 0 the growth of the cells are limited within a duct and have not affected the surrounding tissues. In stage 1, the size of the tumour is 2 centimetres, but lymph nodes are not affected. In stage 2, a tumour sizes is 2 cm and nodes are invaded. In stage 3, a tumour sizes is 5 cm and spreads to lymph nodes. In stage 4 most of the parts are affected.

A study says every woman by age 30 should have mammogram screening to a risk assessment breast cancer. A mammography is a screening technique to identify the symptoms of tumour that cannot be felt. The MIAS is a part of UK research group which has generated a database of mammograms to support and boost researchers' society. It contains 322 digitized mammogram images [15]. The size of the images are1024X1024.The proposed method segments the anomalous area using mutual information. Wirth Michael A., and Alexei Stapinski [28] depicts the use of dynamic shapes. The dynamic shapes can be utilized to extricate the bosom district in mammograms. Breast shape is one of the biggest single highlights of mammogram. Digital mammogram encompasses artifacts in the background. These artifacts are noises in the image [22]. Gaussian noise, salt and pepper, Quantum noise and speckle noise are the noises that are commonly found in mammogram images. The presence of noise influences the ability of classification task and it is a challenging task for experts to make a decision. Overall accuracy of classification methods are decreased significantly with increasing rate of noise [21] in mammography.

The paper is organized as follows. Section II discusses about the related work of previous papers in the same topic. The methods and materials used for this research are discussed in section III. The experimental results of the work carried out for segmenting affected regions are explained in section IV. Finally, section V concludes the research work.

II. LITERATURE SURVEY

Most part of Mammogram division includes characterizing mammograms into a few particular areas, including the bosom fringe, the areola and the pectoral muscle. The important part on a mammogram is the breast outskirt, also called the skin-air interface, or bosom limit. The breast form can be acquired by segmenting the mammogram into breast and non-breast areas. The extracted breast contour should adequately model the soft-tissue/air interface and preserve the nipple in profile.Edge identification is a basic technique of segmentation which shows a sharp change in intensity values. Serhat Özekes et al[23] detected masses using template compared with pixels from region of interest. Different threshold values are used. Similarity was grouped using two thresholds. The results showed sensitivity 93%,

Revised Manuscript Received on July 05, 2019.
  M.P. Sukassini, Research Scholar, BharathiarUniversity, Coimbatore, India.
  T.Velmurugan, Associate Professor, PG and Research Department of Computer Science, D. G. Vaishnav College, Arumbakkam, Chennai-600106, India.

90% and 81% with template diameter 10, 20 and 30 pixels. Greeshma Gopal and Grace Mary Kanaga [8] depict the use of dynamic shapes. The dynamic shapes can be utilized to extricate the bosom district in mammograms. Breast shape is one of the biggest single highlights of mammogram. Indra Kanta Maitra et al [11] proposed automated segment algorithm and boundary detection method to extract breast region. Three methods are combined to segment the breast area. The accuracy estimated based on completeness, correctness and quality which showed 99.4, %99.1% and 99.2%.

Subash Chandra Boss et al [24], proposed a segmentation technique using rough K-Means algorithm. GLCM is used for extracting 14 haralick features of different angles. The features are clustered using kmeans, FCM and RKM to segment ROI. RKM showed better performance. Ibrahim Mohamed Jaber A lamin et al [10] proposed an improved region growing method based on orientation constrain and intensity constrain. The input image is pre-processed using average and laplacian filters. The quality of segmented output is measured using MSE and PSNR. Pappas [26], used the basic k-means clustering technique for segmenting images which has smooth surface objects. Gibbs random field is used as parameters to model shape and size of the regions. It considers spatial constrain and local intensity. The method is tested with faces, optical characters, buildings etc. K-means clustering extracts the pixels into the different clusters as segment. The proposed method showed better performance and fast execution than kmeans.

Sahil Suri et al [20] analysed how speckle noise affects the performance of Scale Invariant feature transform (SIFT) for synthetic aperture radar (SAR) images. SAR image captured at different incidence angles by different sensors and directions are used as input data. Results highlight the efficiency of SIFT for point matching. Nameirakpam Dhanachandra et al [17] used kmeans clustering to segment infected blood cells. The centroid is initiated by subtractive cluster. Contrast stretching is used as pre-processing to progress the quality of input image. Median filter is used as post processing technique to increase the quality of output image. RMSE (Root Mean Square error) and PSNR (Peak-to-Signal Noise Ratio) is used measure the performance which showed better result.

Ng, H. P et al [18] proposed an integrated segment method using kmeans and improved watershed segmentation. The MRI of brain is used as input data. The performance is measured by segmentation maps which has 92%. The partition is lesser than watershed algorithm. Aqil SM Burney and Humera Tariq [3] analysed the performance of kmeans algorithm segmentation in colour space. The number of clusters used was 2, 3 and greater than 3. L*a*b* color space showed the accuracy ranges from 30% to 65% whereas RGB space falls between 30% and 55%. Alpert and Weizmann horse database is used for cluster 2 and 3. Use Berkeley segmentation database is used for more than three clusters.

Georgia D Tourassi et al [7] developed CAD system to detect masses using ROI template with ground truth. The mutual information is used for matching template. Digital Database for Screening Mammography dataset is used. The performance was measured using Receiver operating Characteristics analysis and leaves one out sampling. CAD performance showed as high as Az50.8760.01.Min Dong et al [16] developed a novel automated segment and classification method. ROI is extracted using chain codes and enhanced using rough set. Mass region is extracted by vector field convolution snake (VFC). 32 features were extracted and used as input for different classification. Novel method use random forest. Performance is compared with genetic algorithm SVM, particle swarm optimization SVM, Support Vector Machine and decision tree. The 97.73% accuracy rate is achieved .Matthew's correlation coefficient (MCC) indicator showed 0.8668 and 0.8652 for DDSM and MIAS datasets.

Xiaoming Liu and Zhigang Zeng [29] proposed an automatic detection method. An adaptive region growing method is used to locate suspicious regions. Narrow band based active contour was used to refine the initial regions to improvise accuracy. Gray level co-occurrence matrix and completed local binary pattern was used to extract texture features. SVM was used for classification. MCL showed 82.4% sensitivity with 5.3 false positives per image at masses. After active contour refinement, feature analysis and classification, it showed 78.2% of sensitivity with 1.48FPsI. After classification normal images, MCL showed 5.18 FPsI and 1.51 FPsI. Medio lateral oblique (MLO) images revealed sensitivity 75.6% at 1.38 FPsI. Anan Banharnsakun and Supannee Tanathong [1] Proposed a modified version of Artificial Bee Colony, named as Best-so-far ABC. Template matching is used for object detection. The objective function is based on template objects. The proposed method achieved success in object detection. It also showed optimizing time to reach the solution. Peter Filev et al [19] analysed the performance of similarity measures based on criteria. Euclidean distance, 50% overlap, 75% overlap and similarity measures. Pearsons, cosine and Goodman and Kruskals gamma showed high accuracy.

Hong Yao et al [9] proposed an improved kmeans clustering algorithm for fish image segmentation. Using histogram peaks the best clusters are detected .Otsu method is used to filter the clusters center. Morphology operation is applied to identify the contour. The method showed better results. Jichao Jiao et al [12] proposed a fast template matching algorithm, based on principal orientation difference feature. Edge direction was identified and different features are extracted from template. The method is tested on video. It achieved 95% matching rate. Mahalakshmi and Velmurugan [14] segmented mammogram image using particle swarm optimization technique with multilevel threshold. The output segmented at level three achieved better results and execution time is estimated.

III. METHODOLOGY

The mammography is the best system for an early analysis of the bosom tumour. Finding an exact and productive bosom locale division strategy still remains a testing issue in computerized mammography. Mammogram division as a rule includes ordering mammograms into a few unmistakable areas,

Retrieval Number: I8416078919/19©BEIESP
DOI:10.35940/ijitee.I8416.078919

1862

Published By:
Blue Eyes Intelligence Engineering
& Sciences Publication

including the bosom fringe the areola and the pectoral muscle. The important part on a mammogram is the breast fringe, also called the skin-air interface, or bosom limit. The bosom form can be gotten by apportioning the mammogram into breast and non-bosom locales.

A. Local Map View Technique

The LMV algorithm demonstrates the segmentation of the mammogram images with the various segmentation and clustering possibilities with the images that is to be reached in the way to its boundary and its specified region in the mapping and its consistency to the various indexes and edge with the unique specification of images.

LMV Pseudo code

Let M = {M1,…, Mi ,…, MN} be a matrix of size K × N, where K and N are number of templates and the number of voxels. In this matrix, Mi = [Mi1,…,Mij,…, MiJ]′ and Mij is the label of the template j at voxel i.

Step 1: For all images Mi from initial boundary to destination boundary
Step 2: While Mi has exactly one edge do
    edge e = k. edge (Ke);
    e. level = k.map;
    detect edge e;

Step 3: if (Mij is not the connected region)
    Mi -.Mij> (e$_i$. edge level)
Step 4: View the sub region of edge map e1
    else e. boundary = min(e. region+ 1 -τ,e.edge level);
Step 5: For all indexes i form Mi.........Mij
Step 6: While n has exactly one child do
    Initial Mi= Mij.map (e);
    e. edge= e. region;
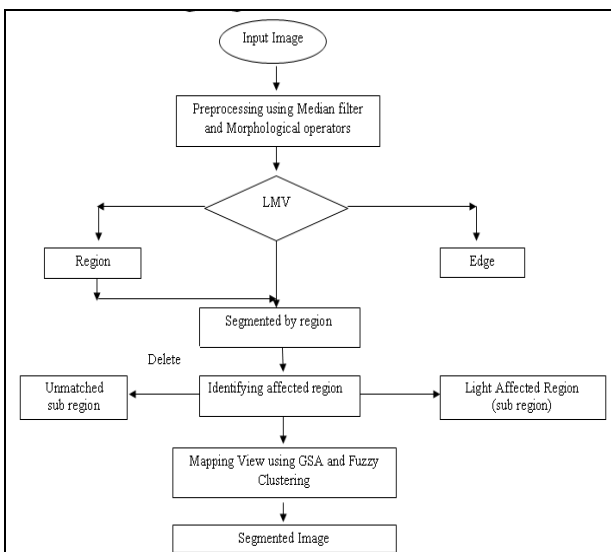   Delete unmatched sub region;
    Correct point map (Mi,e);

Figure1: Architecture diagram of GSLMV

The unmatched boundary region is neglected and the unmatched region is detected by the similarity of the images and the specific region is mapped in mammogram. The mapping is implemented using basic clustering technique. Cluster is comprised of a number of similar objects grouped together based on certain characteristics such as density of data points, distance between the points etc[2]. In this work, Fuzzy Clustering (FCM) is implemented to group the pixels. The algorithm for FCM is

1. Initialize the fuzzy centroids for the clusters.
2. Calculate the distance between the respective cluster centres Dist = | xi - Cj|
3. Update the fuzzy membership based on the distance between the cluster centre and each point in the image/ matrix.

$$U_{ij} = \frac{1}{\sum_{k=1}^{c} \left(\frac{\|x_i - c_j\|}{\|x_i - c_k\|} \right)^{\frac{2}{m-1}}}$$

(1)

4. Calculate the centroid from the updated matrix

$$c_j = \frac{\sum_{i=1}^{N} U_{ij}^{m} \cdot x_i}{\sum_{i=1}^{N} U_{ij}^{m}}$$

(2)

FCM is an iterative process. The termination of FCM depends upon the number of iteration or objective function is less than the predefined convergence value (ε). LMV algorithm reduced the noise rate in segmented output. The performance of LMV regarding noises is recorded.

In our previous work, multilevel threshold and Gravitational Search Algorithm (GSA) was implemented to segment abnormal regions [27]. GSA method was proposed by Esmat Rashedi and Hossein Nezamabadi [4][5] based on Newton's gravity force. The segmentation is based on region and threshold. The threshold level value is initialised as 4, from which three maximum optimal threshold values t1, t2 and t3 (level-1) were calculated using GSA method. The resultant images are formed by mapping optimal threshold values and original input image pixel values. The output image contains three regions mapped from three optimal threshold values. The mapping of pixels is based on threshold, so maximization is considered for calculation of agent's fitness value. The disadvantage of the method is, it reduces the noise to a very low rate.

The second proposed method GSLMV which segments the brighter regions from the input image. In LMV method, the FCM is used to cluster the pixels. FCM performance can be improved by using optimisation techniques. Membership function can be optimised and initializations of cluster centres can use optimised value [13]. The optimal thresholds obtained from GSA method are assigned as initial cluster centres. This modification reduced the execution time of LMV algorithm. The runtime of GSLMV is observed and it is compared with GSA and LMV methods. Since the work is not dealing with classification techniques the pectoral muscle is retained as it is in the segmented image

B. PSNR

The quality of segmented image can be evaluated using various metrics. The jaccard, dice, SSIM and PSNR are some of the metrics used to assess the quality of segmented image. PSNR block computes the peak signal-to-noise ratio, in decibels, between two images. PSNR is calculated using the following equation

$$MSE = \frac{1}{mn} \sum_{i=0}^{m-1} \sum_{j=0}^{n-1} [I(i,j) - K(i,j)]^2 \quad (3)$$

where I(i,j) is the original image, m and n are the row and column of the image and K is the restored image

$$PSNR = 10 \log_{10}\left(\frac{MAX^2}{MSE}\right) \quad (4)$$

where MAX is the maximum intensity of the image. MSE is a mean squared error which represents cumulative squared error between two images

C.FRR

FRR is the false rejection rate which achieves the detection of false regions in the image. The following formula is used to calculate the FRR of the segmented output image.

$$FRR = \frac{Iw - Scw}{Iw} \quad (5)$$

where Iw is the number of white pixels(in voxel) in the input image, Scw is the number of common white pixels(in voxel) from the segmented output image. The common white pixel Scw is identified by performing AND between input image and segmented output image.

IV. RESULTS AND DISCUSSION

The segmentation of abnormal regions in medical image is a challenging work. Various methods are developed to show the identification of brighter regions. GSLMV algorithm is proposed to detect the brighter areas in the cancerous and non cancerous images. These brighter regions are considered as abnormal region in both the categories of images.
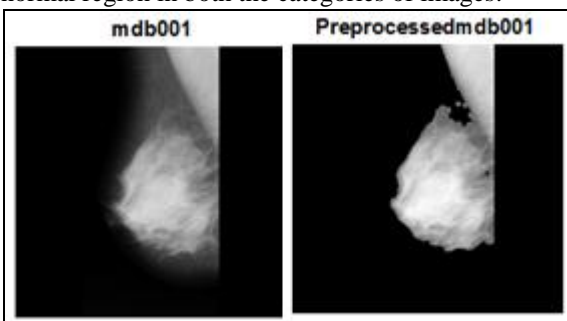

Figure 1: Input image and pre-processed image of mdb001

Different view of mdb001 mammogram image is shown. The figure 1 is the input image from above mentioned dataset and the pre-processed image. Figure 2 shows the three index cluster.
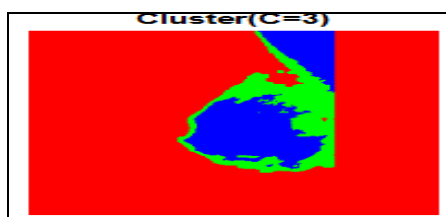

Figure 2: mdb001

The figure 3 establishes the mapping indexes in the various forms by the efficient level of the segmented view with the GSLMV initial segmentation. Those 3 images are now considered as input. This images are again given as feedback data and the following steps are need to proceeded -1) initial background foreground separation, 2)Pixel intensity contrast correlation calculation 3) Based on step 2 neighbour data and position calculation 4) from that position just segmenting thinned layer of abnormal area with the approximate valuation in the image.
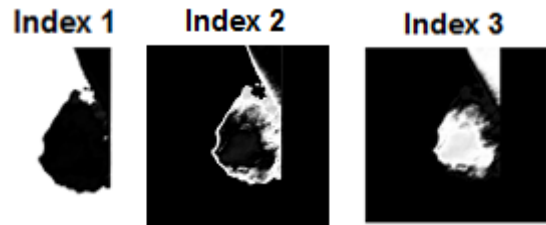

Figure 3: Various views of mapping index of the mdb001

Mapping the images based on the number of groups available for the images and thus achieved doing the low mapping algorithm in the grouped images. Figure 4 shows the mapping index of the segmented image by the experimental analysis.

Figure 4: Segmented brighter regions of mdb001

The GSLMV technique is tested with MIAS dataset. The dataset contains three categories of mammogram images. Fatty, Fatty Grandular and Dense Grandular images. Five samples from each category are tested using GSA, LMV and GSLMV algorithms and the results are tabulated. Table 1 shows the FRR results achieved using equation 5 for fatty mammogram as input images.

Table 1: FRR Results of LMV Method for fatty image

S.No	Input image	No of white Pixels Iw	No of common white pixels Scw	False White pixels Iw – Scw	FRR
1.	mdb012	3177027	19885	3157142	0.9937
2.	mdb028	3722371	25556	3696815	0.9937
3.	mdb070	3825694	21730	3803964	0.9943
4.	mdb098	5468571	27728	5440843	0.9949
5.	mdb148	4245779	29119	4216660	0.9931

1864

The variations in the FRR values of fatty images are very small. The mdb098 shows high value 0.9949 and mdb148 achieved low value 0.9931. Table 2 shows the FRR values of fatty mammograms assessed by GSA method.

Table 2: FRR Results of GSA Method for fatty images

S.No	Input image	No of white Pixels Iw	No of common white pixels Scw	False White pixels Iw – Scw	FRR
1.	mdb012	3177027	19304	3157723	0.9939
2.	mdb028	3722371	25175	3697196	0.9932
3.	mdb070	3825694	21216	3804475	0.9945
4.	mdb098	5468571	27240	5441331	0.9950
5.	mdb148	4245779	28413	4217366	0.9933

There are minor variations in the common white pixels count. Common white pixel count achieved by LMV method is more than GSA. Due to less difference in white pixel count, the FRR accuracy rate between LMV and GSA are very close to each other.

Table 3: FRR Results of LMV Method for fatty grandular images

S.No	Input image	No of white Pixels Iw	No of common white pixels Scw	False White pixels Iw – Scw	FRR
1.	mdb001	2337214	13308	2323906	0.9943
2.	mdb002	2690601	15870	2674731	0.9941
3.	mdb042	3071404	18873	3052531	0.9938
4.	mdb074	2120454	12669	2107785	0.9940
5.	mdb214	2230166	13667	2216499	0.9939

Table 3 shows the FRR values of fatty grandular images assessed by LMV algorithm. The mdb001 achieved high value 0.9943 and mdb042 has low value 0.9938. Table 4 shows the FRR values of fatty grandular mammograms assessed by GSA method

Table 4: FRR Results of GSA Method for fatty grandular images

S.No	Input image	No of white Pixels Iw	No of common white pixels Scw	False White pixels Iw – Scw	FRR
1.	mdb001	2337214	12839	2324375	0.9945
2.	mdb002	2690601	15343	2675258	0.9943
3.	mdb042	3071404	18349	3053055	0.9940
4.	mdb074	2120454	12265	2108189	0.9942
5.	mdb214	2230166	13155	2217011	0.9941

The sample image mdb001 yielded high value 0.9945 and mdb042 has low value 0.9940. The common white pixel count yielded by LMV is more than GSA. Due to small difference in the count, the FRR of LMV algorithm is close to

GSA method.

Table 5: FRR Results of LMV Method for dense grandular images

S.No	Input image	No of white Pixels Iw	No of common white pixels Scw	False White pixels Iw – Scw	FRR
1.	mdb058	3738905	21319	3717586	0.9942
2.	mdb063	3217149	17851	3199298	0.9944
3.	mdb100	3203645	19907	3183738	0.9937
4.	mdb101	2789569	15997	2773572	0.9942
5.	mdb145	4392009	28864	4363145	0.9934

Table 5 shows the FRR values of dense grandular mammogram as input images by LMV technique. Mdb063 achieved high FRR value 0.9942 and mdb145 achieved 0.9934. Table 6 shows the FRR values of dense mammograms assessed by GSA method.

Table 6: FRR Results of GSA Method for dense grandular images

S.No	Input image	No of white Pixels Iw	No of common white pixels Scw	False White pixels Iw – Scw	FRR
1.	mdb058	3738905	20910	3717995	0.9944
2.	mdb063	3217149	17512	3199637	0.9946
3.	mdb100	3203645	18517	3185128	0.9942
4.	mdb101	2789569	15674	2773895	0.9944
5.	mdb145	4392009	28277	4363732	0.9936

Table 6 shows that mdb063 has the FRR value as 0.9946 and mdb145 has 0.9936. Analysing table 5 and 6, LMV method identified more number of common white pixel count than GSA. The FRR rate of LMV and GSA are very close to each other. The table 1, 2,3,4,5 and 6 shows that common pixel determined by LMV algorithm is greater than that of GSA. Due to less count of common pixel by GSA, there is increase in FRR of GSA. Samples of different categories showed 99% of false rejection rate by LMV and GSA. Since accuracy rate of LMV and GSA are very close, it is very difficult to analyse the performance of LMV. The GSLMV is implemented to segment the abnormal regions and false rejection rate is calculated.

Table 7: FRR Results of GSLMV Method for fatty images

S.No	Input image	No of white Pixels Iw	No of common white pixels Scw	False White pixels Iw – Scw	FRR
1.	mdb012	3177027	19885	3157142	0.9937
2.	mdb028	3722371	25556	3696815	0.9937
3.	mdb070	3825694	21730	3803964	0.9943
4.	mdb098	5468571	27728	5440843	0.9949
5.	mdb148	4245779	29119	4216660	0.9931

The results of FRR determined by GSLMV is tabulated in table 7,8 and 9 for fatty, fatty grandular and dense grandular images. This method showed same FRR accuracy rate as LMV method. The common white pixels count is also same as LMV method.

Table 8: FRR Results of GSLMV Method for fatty grandular images

S.No	Input image	No of white Pixels Iw	No of common white pixels Scw	False White pixels Iw – Scw	FRR
1.	mdb001	2337214	13308	2323906	0.9943
2.	mdb002	2690601	15870	2674731	0.9941
3.	mdb042	3071404	18873	3052531	0.9938
4.	mdb074	2120454	12669	2107785	0.9940
5.	mdb214	2230166	13667	2216499	0.9939

Three categories of mammogram showed the same count because the integration of fitness values is implemented only for clustering of pixels to form segmented image. PSNR metric is used to analyse the GSA, LMV and GSLMV algorithm performance.

Table 9: FRR Results of GSLMV Method for dense grandular images

S.No	Input image	No of white Pixels Iw	No of common white pixels Scw	False White pixels Iw – Scw	FRR
1.	mdb058	3738905	21319	3717586	0.9942
2.	mdb063	3217149	17851	3199298	0.9944
3.	mdb100	3203645	19907	3183738	0.9937
4.	mdb101	2789569	15997	2773572	0.9942
5.	mdb145	4392009	28864	4363145	0.9934

The PSNR is evaluated using equation 4. The results are tabulated for three categories of mammogram. PSNR values of resultant segmented images by GSA, LMV and GSLMV techniques are tabulated

Table 10(a): PSNR and Relative Increase for Fatty Images

S. No	Image	PSNR			
		Input image(I)	GSA	LMV	GSLMV
1.	mdb012	12.1458	30.3125	79.149	79.149
2.	mdb028	24.6579	28.8478	79.496	79.496
3.	mdb070	25.4305	29.9769	79.584	79.584
4.	mdb098	26.2242	29.8430	78.9246	78.9246
5.	mdb148	15.7317	28.3446	81.2918	81.2918

Table 10(b): PSNR and Relative Increase for Fatty Images

S. No	Image	Relative Increase in PSNR		
		GSA-I	LMV-I	GSLMV-I
1.	mdb012	+18.1667	+67.0032	+67.0032
2.	mdb028	+4.1899	+54.8381	+54.8381
3.	mdb070	+4.5464	+54.1535	+54.1535
4.	mdb098	+3.6188	+52.7004	+52.7004
5.	mdb148	+12.6129	+65.5601	+65.5601

The relative increase represents the difference value of PSNR between the input images (I) and the segmented images by GSA, LMV and GSLMV methods. The relative difference of GSA is less than LMV and GSLMV. Higher the increase in relative difference shows that LMV and GSLMV removed more noises from the image. The quality of segmented image by LMV and GSLMV is better than GSA, but the segmented image of LMV and GSLMV has shown same PSNR value. That shows the output of LMV and GSLMV are of same quality. So, runtime of the entire three algorithms is taken as a metric measure. The execution time of the each algorithm for three categories of mammogram is tabulated. The runtime of each method is repeatedly observeed and average runtime is calculated.
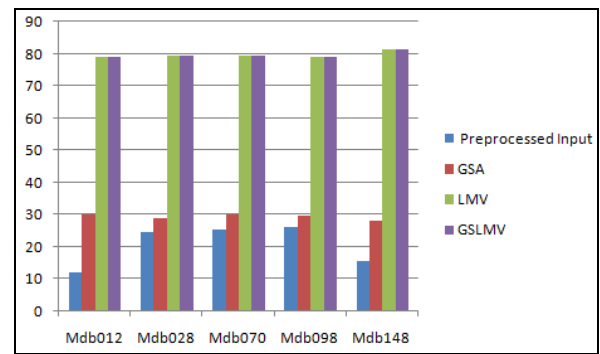

Figure 4. Comparison of PSNR results for fatty images

Figure 4 shows the drastic change in PSNR values of three algorithms. The runtime parameter of fatty images is recorded in table 11.

Table 11 : Runtime of Fatty Images

S. No	Image	GSA(sec)	LMV(sec)	GSLMV(sec)
1.	mdb012	12.3913	4.6402	3.4532
2.	mdb028	22.9819	3.6794	3.1132
3.	mdb070	12.8684	3.2497	2.9241
4.	mdb098	16.7018	2.2367	2.0132
5.	mdb148	10.4548	3.5291	3.1866

Analysing table 11, the runtime of GSA is higher than LMV and GSLMV algorithm. Difference in runtime of LMV and GSLMV is small. GSLMV showed lesser runtime than the other two methods.
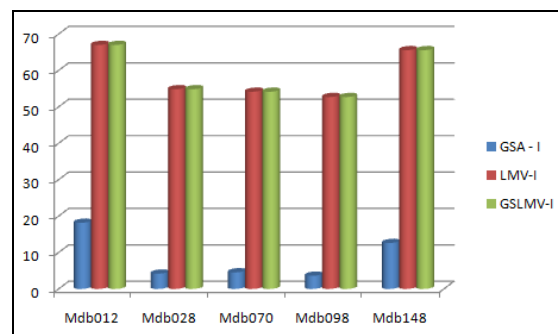

Figure 5. Relative increase of PSNR values for fatty images

Table 12 shows the quality of segmented output image by LMV and GSLMV which is better than GSA.

Table 12(a): PSNR and Relative Increase for fatty grandular

S.No	Input image	PSNR			
		Input Image(I)	GSA	LMV	GSLMV
1.	mdb001	22.5127	31.7448	80.7511	80.7511
2.	mdb002	17.4208	31.0577	80.1880	80.1880
3.	mdb042	19.6935	30.6145	79.7482	79.7482
4.	mdb074	25.4078	31.9367	79.7912	79.7912
5.	mdb214	24.8665	31.7710	78.9059	78.9059

Table 12(b): PSNR and Relative Increase for fatty grandular

S.No	Input image	Relative Increase in PSNR		
		GSA-I	LMV - I	GSLMV-I
1.	mdb001	+9.2321	+58.2384	+58.2384
2.	mdb002	+13.6369	+62.7672	+62.7672
3.	mdb042	+10.9210	+60.0547	+60.0547
4.	mdb074	+6.5289	+54.3834	+54.3834
5.	mdb214	+6.9045	+54.0394	+54.0394

The segmented output image of LMV and GSLMV has shown same PSNR value. That shows the output of LMV and GSLMV are of same quality

Table 13: Runtime of Fatty Grandular Images

S. No	Image	GSA(sec)	LMV(sec)	GSLMV(sec)
1.	mdb001	18.4035	4.5237	2.5218
2.	mdb002	12.4111	3.3881	2.9801
3.	mdb042	17.1168	4.0814	3.2513
4.	mdb074	10.8508	3.3503	3.1629
5.	mdb214	10.8237	2.6421	3.3850

Analysing table 13, the runtime of GSA is high than LMV and GSLMV algorithm. GSLMV showed lesser runtime than the other two methods.
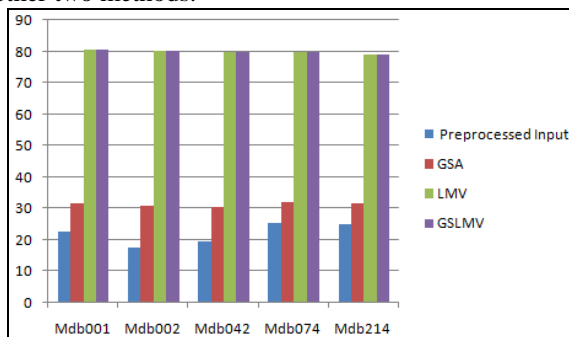

Figure 6. Comparison of PSNR results for fatty grandular images

Figure 6 represents the PSNR value of input image GSA, LMV and GSLMV. There is a drastic increase in PSNR of LMV and GSLMV algorithms.
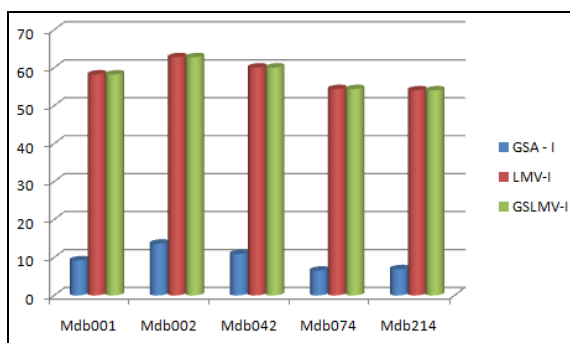

Figure 7. Relative increase of PSNR values for fatty grandular images

Figure 7 shows the relative increase in PSNR of fatty grandular images by GSA, LMV and GSLMV.

Table 14 (a): PSNR and Relative Increase of dense grandular

S. No	Input image	PSNR			
		Input Image(I)	GSA	LMV	GSLMV
1.	mdb058	18.6871	29.8569	78.8432	78.8432
2.	mdb063	19.2196	30.4668	79.0988	79.0988
3.	mdb100	24.7539	30.2820	79.3253	79.3253
4.	mdb101	21.8531	31.0155	79.7468	79.7468
5.	mdb145	11.1464	28.3527	80.6932	80.6932

Table 14 (b): PSNR and Relative Increase of dense grandular

S. No	Input image	Relative Increase in PSNR		
		GSA-I	LMV-I	GSLMV-I
1.	mdb058	+11.1698	+60.1561	+60.1561
2.	mdb063	+11.2472	+50.8792	+50.8792
3.	mdb100	+5.5281	+54.5714	+54.5714
4.	mdb101	+9.1624	+57.8937	+57.8937
5.	mdb145	+17.2063	+69.5468	+69.5468

Table 14 shows the PSNR value segmented output image by LMV and GSLMV. The quality of output image obtained by LMV and GSLMV is better than GSA. The PSNR of segmented output image of LMV and GSLMV is shown same. That shows the output of LMV and GSLMV are of same quality.
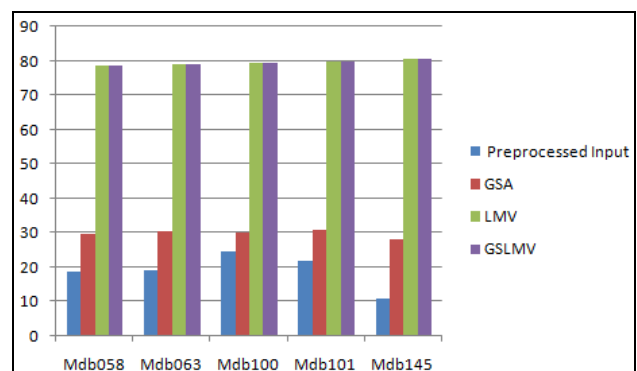

Figure 8. Comparison of PSNR results for dense grandular images

Increase in PSNR value of dense grandular images is represented by graph in figure 8.

Table 15: Runtime of dense grandular Images

S.No	Image	GSA(sec)	LMV(sec)	GSLMV(sec)
1.	mdb058	20.6951	3.5962	2.7488
2.	mdb063	10.4482	3.1980	3.1352
3.	mdb100	11.0211	2.9383	2.8130
4.	mdb101	14.6345	3.0111	3.3415
5.	mdb145	16.5583	3.7892	2.3803

Analysing table 15, the runtime of GSA is more than LMV and GSLMV algorithm. GSLMV showed lesser runtime than the other two methods for dense grandular images.
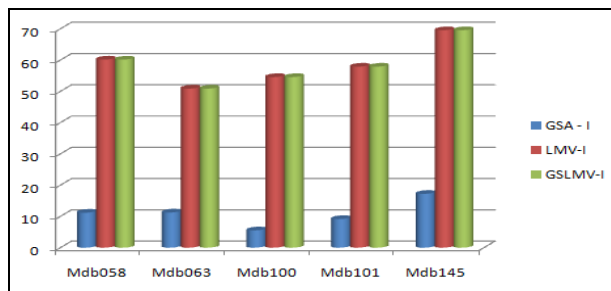
Figure 9. Relative increase of PSNR values for dense grandular images

Figure 9 shows the graphical representation of relative increase of PSNR for dense grandular samples.

V. CONCLUSION

The tracing of abnormal regions in mammogram image supports the radiologist to fix on the phase of the ailment in women. The characteristics of the various segmentation process and their functionalities in the mammogram images have their different respective principles. Some segmentation methods identify the larger region and miss the smaller areas which have the possibilities of cancer. The proposed GSLMV technique groups the comparative similarity pixels and their positions are identified which is more efficiently used in segmenting mammogram images. The local quality of each point in all instances of the region is also determined. The accuracy of GSLMV is determined using false rejection rate, pixel count. PSNR and runtime metrics. False rejection rate of GSLMV is compared with GSA and LMV algorithms which showed very less variation due to common pixel count. All the three methods obtained approximately 99% of FRR. PSNR is used to estimate the quality of segmented output image of GSA, LMV and GSLMV. LMV and GSLMV showed increasing rate of PSNR value than GSA. Runtime parameter is used to measure the robustness performance of the GSLMV with GSA and LMV method. The runtime of GSLMV is less than that of GSA and LMV. Based on the white pixel count, runtime and PSNR metrics our proposed method is better than GSA and taking into account of runtime GSLMV is better than LMV.

REFERENCES

1. Anan Banharnsakun and SupanneeTanathong, "Object detection based on template matching through use of best-so-far ABC", Computational intelligence and neuroscience, Vol. 7, 2014.
2. Anil K Jain and Richard C. Dubes, "Algorithms for clustering data", 1988.
3. Aqil Burney S.M and Humera Tariq, "K-means cluster analysis for image segmentation", International Journal of Computer Applications, Vol. 96, 2014.
4. Esmat Rashedi, Hossein Nezamabadi-Pour and Saeid Saryazd," GSA: a gravitational search algorithm", Information sciences, Vol. 13, pp. 2232-2248, 2009.
5. Esmat Rashedi and Hossein Nezamabadi-Pour, "A stochastic gravitational approach to feature based color image segmentation", Engineering Applications of Artificial Intelligence, Vol. 4, pp. 1322-1332, 2013.
6. Gonzalez Rafael C. Digital image processing, Pearson Education India, Third Edition., 2009.
7. Georgia D Tourassi, Rene Vargas-Voracek, David M. Catarious and Carey E. Floyd, "Computer assisted detection of mammographic masses a template matching scheme based on mutual information. Medical physics, Vol. 30, pp. 2123-2130, 2003.
8. Greeshma Gopal and E. Grace Mary Kanaga, " A Study on Enhancement Techniques for Mammogram Images", International Journal of Advanced Research in Electronics and Communication Engineering, Vol. 2, 2013.
9. Hong Yao, QinglingDuan, Daoliang Li and Jianping Wang, "An improved K-means clustering algorithm for fish image segmentation", Mathematical and Computer Modelling, Vol. 58, pp. 790-798, 2013.
10. Ibrahim Mohamed Jaber Alamin, W. Jeberson and H. K. Bajaj, "Improved Region Growing based Breast Cancer Image Segmentation", International Journal of Computer Applications, Vol. 135, 2016.
11. Indra Kanta Maitra, Sanjay Nag and Samir K. Bandyopadhyay," Accurate breast contour detection algorithm in digital mammogram", International Journal of Computer Applications Vol. 25, pp. 1-13, 2011.
12. Jichao Jiao, Xin Wang, Zhongliang Deng, Jichang Cao and Weihua Tang, " A fast template matching algorithm based on principal orientation difference", International Journal of Advanced Robotic Systems, Vol. 15, 2018.
13. Kumar, S. N., A. Lenin Fred, H. Ajay Kumar, and P. Sebastin Varghese, "Firefly Optimization Based Improved Fuzzy Clustering for CT/MR Image Segmentation", Nature Inspired Optimization Techniques for Image Processing Applications, Springer, pp. 1-28, 2019.
14. Mahalakshmi and T. Velmurugan, " Detection of brain tumour by particle swarm optimization using image segmentation", Indian Journal of Science and Technology,Vol.8, pp.13-19,2015
15. Mammographic Image Analysis Societyhttp://peipa.essex.ac.uk/info/mias.html.
16. Min Dong, Xiangyu Lu, Yide Ma, YananGuo, Yurun Ma and Keju Wang, "An efficient approach for automated mass segmentation and classification in mammograms", Journal of digital imaging, Vol. 28, pp. 613-625, 2015.
17. Nameirakpam Dhanachandra, Khumanthem Manglem and Yambem Jina Chanu,"Image segmentation using K-means clustering algorithm and subtractive clustering algorithm", Proceedia Computer Science, Vol. 54, pp. 764-771, 2015.
18. Ng, H. P., S. H. Ong, K. W. C. Foong, P. S. Goh and W. L. Nowinski, " Medical image segmentation using k-means clustering and improved watershed algorithm", Image analysis and Interpretation, IEEE, pp. 61-65, 2006.
19. Peter Filev, LubomirHadjiiski, BerkmanSahiner, Heang-Ping Chan and Mark A. Helvie, Comparison of similarity measures for the task of template matching of masses on serial Mammograms", Medical physics, Vol.32, pp. 515-529, 2005.
20. Sahil Suri, Peter Schwind, Johannes Uhl and Peter Reinartz, "Modifications in the SIFT operator for effective SAR image matching", International Journal of Image and Data Fusion, Vol. 1, pp. 243-256, 2010.
21. Saima Anwar Lashari, Rosziati Ibrahim and Norhalina Senan, "Wavelet threshold de-noising for mammogram images", International Journal of Software Engineering and Its Application Vol. 6,pp. 215-226, 2015.
22. Sara Dehghani and Mashallah Abbasi Dezfooli, "A method for improve preprocessing images mammography," International Journal of Information and Education Technology,Vol. 1, pp. 90, 2011.
23. Dharmarajan, K., and M. A. Dorairangaswamy. "Discovering Student E-Learning Preferred Navigation Paths Using Selection Page and Time Preference Algorithm." International Journal of Emerging Technologies in Learning (iJET) 12.10 (2017): 202-211.
24. Subash Chandra Boss R, K. Thangavel and D. A. Daniel, "Mammogram image segmentation using rough clustering", International Journal of Research in Engineering and Technology, Vol. 2, pp. 66-77, 2013.
25. Sukassini M.P and Velmurugan T, "Noise removal using Morphology and Median filter Methods in Mammogram Images", 3rd International Conference on Small & Medium Business Vietnam, 2016.
26. Thrasyvoulos N Pappas, "An adaptive clustering algorithm for image segmentation", IEEE Transactions on signal processing, Vol. 40, pp. 901-914 1992.
27. Velmurugan, T and M. P. Sukassini,"Segmentation of Mammogram Image using Multilevel Threshold and Gravitational Search Algorithm", IJCTA, Vol. 9, pp. 67-75, 2016.
28. Wirth A Michael and Alexei Stapinski, "Segmentation of the breast region in mammogram using active contours", Visual Communications and Image Processing, Vol. 5150, pp.1995-2007.
29. Xiaoming Liu and ZhigangZeng, " A new automatic mass detection method for breast cancer with false positive reduction. Neurocomputing, Vol. 152, pp. 388-402, 2015.